Journal of Solar Energy Research (JSER)

Journal homepage: www.jser.ut.ac.ir

Analysis of Electromagnetic Transient Overvoltages of PV Systems Considering Frequency Dependence of Grounding System

Ali Mehri, Reza Ghanizadeh*, Mojtaba Beiraghi

Department of Electrical Engineering, Urmia Branch, Islamic Azad University, Urmia, Iran

ARTICLE INFO

Article Type:

Research Article

Received:27.04.2023
Accepted:08.09.2023

Keywords:
Grounding systems
photovoltaic systems
soil electrical parameters
wide-band modeling
partial element equivalent-circuit method

A B S T R A C T

Photovoltaic (PV) systems are susceptible to lightning strikes. In this paper, a new accurate and efficient electromagnetic transient (EMT) model of grounding systems (GSs) is presented. The proposed approach considers the impact of frequency-dependent (FD) modeling of GSs on the overvoltage values in PV systems in time domain analysis. The proposed wide-band model is significantly accurate for various types of GSs (single-port and multi-port GSs) and models the frequency dependence of the soil electrical parameters based on experimental data (conductivity and relative permittivity). The proposed model can be implemented in time domain without any GS impedance matrix inversion, so it has less complexity compared to previous approaches. Most of the existing studies suffer from low accuracy in the PV system modeling during lightning transients because of neglecting the effects of the mounting system, metal frame, and mutual coupling, which are considered in the present work. The results demonstrate that the PV factors and frequency dependence of soil have a great effect on the PV system overvoltages. The proposed model offers improved accuracy, by covering the entire frequency range of interest. Additionally, it takes into account the mounting system, metal frame, and mutual coupling in EMT analysis.

1. Introduction

There has been a rapid expansion of renewable energy sources, particularly the combination of solar photovoltaic (PV) and wind turbine generating (WTG) systems, which have drawn much interest in tackling global warming and climate change concerns [1]. These energy sources provide various benefits, including reduced emissions and lower operational costs. However, the power output of PV and WTG systems is uncertain. To address fluctuating energy costs, it is necessary to optimize the scheduling of a microgrid that incorporates diverse energy sources

*Corresponding Author Email: r.ghanizadeh@iaurmia.ac.ir

Cite this article: Mehri, A., Ghanizadeh, R., & beiraghi, M. (2023). Analysis of Electromagnetic Transient Overvoltages of PV Systems Considering Frequency Dependence of Grounding System. Journal of Solar Energy Research, 8(3), 1587-1598. doi: 10.22059/jser.2023.358411.1294

DOI: 10.22059/jser.2023.358411.1294 DOR: 20.1001.1.25883097.2023.8.3.2.2

©The Author(s). Publisher: University of Tehran Press.

[2] and to give due consideration to microgrid protection [3].

Solar PV systems are regarded as one of the best renewable energy resources for substituting conventional energy sources [4]. Different types of grid-connected PV systems have been developed [5] and put into commercial use. Because of recent technological advances, policy encouragement, and high demand, PV systems have expanded extensively worldwide. One way to increase the voltage gain and reduce the voltage stress on the connected switch in PVs is to utilize coupled inductors. In [6], a zero current switching step-up converter is proposed to reduce the voltage stress on the switch.

Like other power systems, PV systems are vulnerable to lightning strikes because they are always installed in unsheltered open areas [7]. It has been reported that an average of 26% of PV system damages is caused by lightning [8]. To analyze the lightning performance of PV systems, an accurate and reliable model of different parts of electromagnetic (EM) circuits, including PV modules and grounding systems, has to be developed [9].

The scientific background of lightning protection system (LPS) design for solar systems and the standardization aspects were discussed in [10-11]. In [12], the transient behavior of a PV system was studied using experimental tests on individual PV modules and reduced-scale models. The lightning performance of a PV system under both direct and indirect lightning strikes was analyzed and compared with the field measurement in [13].

To monitor the terminal voltage of PV modules, high-speed data loggers have been used [14]. A main part of the lightning current passes through the PV system cables, the earth-termination system cables, and surge protection devices, which must be properly designed to protect the entire system, especially the high-price equipment such as inverters [15].

The effects of grounding system (GS) modeling on the lightning protection of PV plants were discussed in [16]. In [17-18], the risk assessment and efficiency of solar systems under different lightning strikes were analyzed. The results showed that the PV efficiency significantly decreases after imposing different lightning strikes on PV modules. In [19], a PV system was implemented based on the Partial Element Equivalent Circuit (PEEC) approach, which uses the equivalent R, L, and C parameters. However, these works did not consider the effect of mutual coupling, so their results were inaccurate.

Most of the above-mentioned studies have low accuracy in PV system modeling under lightning transients due to neglecting the effect of the mounting system, metal frame, and mutual coupling. In these studies, the GS has been modeled as a simple resistance in calculating the lightning overvoltages. In previous investigations on the effects of GS on PV modules, the frequency dependency of soil electrical parameters has been ignored.

In this study, to analyze the effect of wide-band modeling of GS on the PV generated lightning overvoltage, an accurate approach is utilized. This method accurately transforms the impedance matrix of GS from the frequency domain into the time domain. The proposed approach is capable to model both single-port and multi-port GSs. To demonstrate the efficiency of the proposed GS modeling on the lightning performance of PV, some simulations are performed on a test solar system. To decrease the complexity, a straightforward approach is utilized to implement the impedance matrix of the GS in the time domain without matrix inversion. The proposed approach can be summarized as follows: First, the method of moments (MoM) is used to extract the impedance matrix of GS in the lightning frequency range. Second, the vector fitting (VF) method is utilized to transform the impedance matrix into the time domain. Finally, some variable transformations and modifications are made to prepare the frequency dependent impedance matrix of GS for implementation in EMT solvers. Moreover, the PV model considers the effects of the mounting system, metal frame, and mutual coupling on EMT behavior at different points of the PV system. The simulation results of PEEC modeling of PV and frequency-dependent (FD) wide-band modeling of GSs are validated using laboratory test results. The validated results ensures that the proposed models can be applied to large-scale systems. The novelty of the proposed model is higher accuracy in both low and high frequency range of interest, it also offers lower complexity by avoiding inversion of GS impedance matrix, furthermore it can be applied for two-layer soil. Additionally, it takes into account the mounting system, metal frame, and mutual coupling of PV arrays in EMT analysis.

This paper is organized as follows: Section 2 describes the transient modeling of photovoltaic systems. In Section 3, the modeling of GS is explained in detail. The results of this study are presented in Section 4, and finally, Section 5 concludes the paper.

2. Modeling of Photovoltaic system

A photovoltaic module is fixed using an aluminium mounting system, and the lightning

currents discharge through the GS that is connected to the metal mounting system. The main goal of this research is to assess the transient behaviour of PV systems under lightning stroke. The solar system is modeled using the PEEC method, and the GS model is frequency dependent. The PEEC method is one of the accurate methods used to represent the PV system by its equivalent RLC circuit to study lightning transients, as explained in the upcoming section.

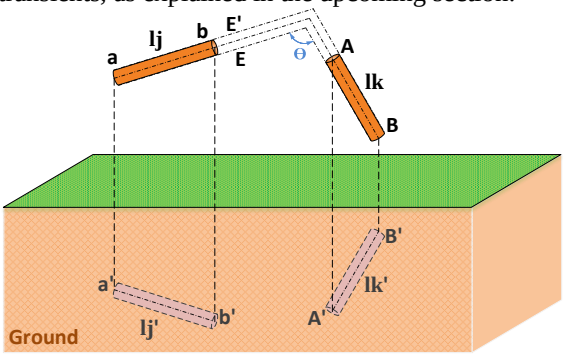

(a)

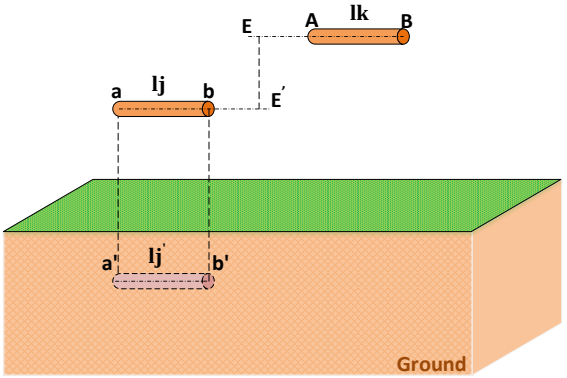

(b)

Figure 1. Conductor's positions. (a) Nonparallel, (b) Parallel

2.1. PEEC Modeling

The main reason for using PEEC in modelling the PV system is to consider the effect of geometry of the mounting system on the potential coefficient matrices. There are two types of conductor arrangement, i.e., parallel and nonparallel, as demonstrated in Figure 1.

The angles and lengths of conductors and the mounting system considered in calculating the potential coefficient matrix are as follows [20]:

$$P_{jk} = \frac{1}{4\pi\varepsilon l_j l_k}(\Lambda_{jk} - \Lambda_{j'k}) \tag{1}$$

where l_j and l_k are the lengths of conductors j and k, respectively. For the nonparallel arrangement, Λ_{jk} is given below [20]:

$$\begin{aligned}\Lambda_{jk} &= \int_{l_k}\int_{l_j}\frac{1}{R_1}dl_j dl_k = (d_2+1)\ln\frac{d_4+d_5+m}{d_4+d_5-m}\\ &-d_2\ln\frac{d_6+d_7+m}{d_6+d_7-m}+(d_3+m)\ln\frac{d_4+d_7+l}{d_4+d_7-l}\\ &-d_3\ln\frac{d_5+d_6+l}{d_5+d_6-l}-\frac{\delta d}{\sin\theta}\end{aligned} \tag{2}$$

where

$$\begin{aligned}\delta &= \tan^{-1}\left(\frac{d_1}{d_4\tan\theta}+\frac{(d_2+l)(d_3+m)\sin\theta}{d_1 d_4}\right)\\ &-\tan^{-1}\left(\frac{d_1}{d_5\tan\theta}+\frac{(d_2+l)d_3\sin\theta}{d_1 d_5}\right)\\ &+\tan^{-1}\left(\frac{d_1}{d_6\tan\theta}+\frac{d_2 d_3\sin\theta}{d_1 d_6}\right)\\ &-\tan^{-1}\left(\frac{d_1}{d_7\tan\theta}+\frac{d_2(d_3+m)\sin\theta}{d_1 d_7}\right)\end{aligned} \tag{3}$$

where d_1, d_2, d_3, d_4, d_5, d_6, and d_7 are the lengths of respectively lines *E'E*, *EA*, *E'a*, *Bb*, *Ba*, *Aa*, and *Ab* shown in Figure 1 (a). For the parallel arrangement, Λ_{jk} is expressed as [20]:

$$\begin{aligned}\Lambda_{jk} &= (l+d_9+m)sinh^{-1}\frac{l+d_9+m}{d_8}\\ &-\sqrt{(l+d_9+m)^2+d_8^2}+d_9 sinh^{-1}\frac{d_9}{d_8}-\sqrt{d_8^2+d_9^2}\\ &-(m+d_9)sinh^{-1}\frac{m+d_9}{d_8}+\sqrt{(m+d_9)^2+d_8^2}\\ &-(l+d_9)sinh^{-1}\frac{l+d_9}{d_8}+\sqrt{(l+d_9)^2+d_8^2}\end{aligned} \tag{4}$$

where d_8 and d_9 are, respectively, the lengths of lines *Eb* and *AE*.

Considering *n* positive coupling branch conductor units for the PV frame, the equivalent capacitance and inductance matrices are given below [20]:

$$\begin{aligned}&C_{jj} = \sum_{i=1}^{n} P_{jk}\,(j=1,2,3,.....,k,.....,n-1,n)\\ &C_{jk} = -P_{jk}\,(j,k=1,2,3,.....,n)k\neq j\\ &L = \mu_o\varepsilon_o C^{-1}\end{aligned} \tag{5}$$

where P is the potential coefficient matrix, μ_0 and ε_0 are, respectively, the permeability and permittivity of vacuum. The resistance can be expressed as [21]:

$$R_i = \frac{l_i \sqrt{\mu f_c}}{2r\sqrt{\pi\sigma_c}} \quad (6)$$

where i is the conductor number; μ, σ_c, and f_c are the conductor permeability, branch conductivity, and upper cutoff frequency, respectively; l_i and r are, respectively, the length and radius of the conductor. The equivalent π-coupled circuit is extracted using the R, L, and C matrices (Figure 2) [20].

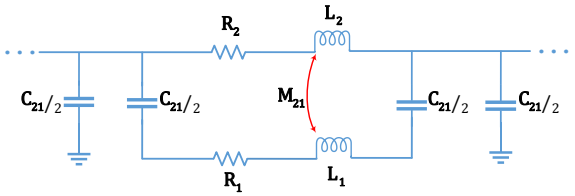

Figure 2. Π-coupled equivalent circuit for two-segment conductor

3. GS modeling

In this paper, two approaches to GS modelling are considered. The first approach is "static model", which employs a simple resistor equivalent to DC resistance. The second approach is "FD wide-band model", which is proposed in the present study. This model considers the frequency-dependency of soil electrical parameters. It should be noted that we ignore the soil ionization in this paper.

The proposed wide-band modeling approach can be summarized as follows:

1. MoM is employed to solve Maxwell equations and calculate the grounding system impedance matrix, considering the desired frequency content.
2. The VF method is utilized to fit a set of residues and poles to all impedance matrix arrays.
3. To enable compatibility with EMT-tools like EMTP, which relies on the admittance matrix, the state-space equations of the grounding systems are derived based on the admittance matrix. This involves applying a variable transformation. The resulting state-space grounding system matrices (A, B, C, and D) can be effectively employed to model different types of grounding systems in various EMT-type solvers.

3.1. MoM modeling

To calculate the impedance matrix of the GS in a frequency range from DC to several MHz, based on the frequency content of lightning currents, the electromagnetic method (MoM) is used.

The current distribution in conductor segments is expressed as [22]:

$$I(l) = \sum_{K=.1}^{K} I_k F_k(l) \quad (7)$$

where $F_k(l)$ is the current distribution along the kth dipole, l is the length of each segment, K is the number of dipoles, and I_k is the unknown current. The GS electric field components are (see further details in [22]):

$$\begin{aligned} E_\rho = {} & \frac{\eta}{4\pi\rho \sinh\gamma\rho}[(I_1 e^{-\gamma R_1} - I_2 e^{-\gamma R_2})sinh\gamma d \\ & + (I_1 cosh\gamma d - I_2)e^{-\gamma R_1}cos\theta_1 \\ & + (I_2 cosh\gamma d - I_1)e^{-\gamma R_2}cos\theta_2] \end{aligned} \quad (8)$$

$$\begin{aligned} E_z = {} & \frac{\eta}{4\pi\rho sinh\gamma d}[(I_1 - I_2 cosh\gamma d)\frac{e^{-\gamma . R_2}}{R_2} \\ & + (I_2 - I_1 cosh\gamma d)\frac{e^{-\gamma R_1}}{R_1}] \end{aligned} \quad (9)$$

$$E_\varphi = 0 \ , \ \eta = \sqrt{\frac{\mu}{\varepsilon}} \quad (10)$$

where η is the intrinsic impedance of the medium, E_ρ, E_z, and E_φ are the components in cylindrical coordinates, and $\gamma=-\omega^2\mu\varepsilon_1$; I_1, and I_2 are the end-point dipole currents.

Impedance matrix $z_{ij}(s)$ is expressed by [22]:

$$Z_{ij} = \left.\frac{V_i(s)}{I_i(s)}\right|_{I_s=0,(s=1,2,3,\ldots,k,s\neq j)} \quad (11)$$

where K is the number of grounding ports. Therefore, the GS impedance matrix is [22]:

$$Z_g(s) = \begin{pmatrix} Z_{11}(s) & \ldots & Z_{1k}(s) \\ \vdots & \ddots & \vdots \\ Z_{.k1}(s) & \ldots & Z_{kk}(s) \end{pmatrix} \quad (12)$$

where Z_{ij} is the mutual-impedance between ports i and j, and Z_{ii} is the self-impedance of the GS.

3.2. Conversion of FD wide-band model of GS into time domain

An improved version of VF method is developed and proved as an efficient iterative scheme for calculating the appropriate poles and residues. The improved VF replaced the old poles with the new ones. The pole-residue model of each vector can be expressed by [23]:

$$z_{ij}(s) \approx \{z_{ij}(s)_{fit}\} = \sum_{m=1}^{M} \frac{R_{m,ij}}{s - a_m} + d_{ij} + se_{ij} \quad (13)$$
$$i = 1,2,\ldots,K;\ j = 1,2,\ldots,K$$

where R_m and a_m are the residues and poles, respectively. K is the number of ports; d and e are constant.

In the proposed method, it is required to have a pure state-space output ($D\neq0$, $E=0$). However, the VF method can result in either a pure or an impure output. To ensure the desired pure output, the approach is to select the pure mode during the modeling process. By specifically choosing the pure mode, it becomes possible to obtain an appropriate output that adheres to the requirement of a pure state-space representation. This selection is crucial in achieving accurate and reliable modeling outcomes (i.e., matrix $D\neq0$).

To have a stable time-domain simulation, passivity should be enforced in the pole-residue model of GS [24]. The impedance matrix pole-residue model can be shown in state-space equation as:

$$\dot{x}(t) = A.x(t) + B.i(t)$$
$$v(t) = C.x(t) + D.i(t) \quad (14)$$

where $x(t)$, $v(t)$, and $i(t)$ are, respectively, the state, voltage, and current vectors related to each port; W is the total number of state variables; $\boldsymbol{A} \in R^{W\times W}$, $\boldsymbol{B} \in R^{W\times K}$, $\boldsymbol{C} \in R^{n\times W}$, $\boldsymbol{D} \in R^{n\times K}$, *and* $\boldsymbol{E} \in R^{n\times K}$.

Implementing the state-space impedance matrix of GS in an EMT-type tool, like EMTP, needs some variable changes. It is worth noting that EMT solvers commonly utilize Dommel's method, which relies on the admittance matrix for simulation purposes. As a result, when the grounding systems are modelled for compatibility with EMT solvers, the state-space matrices should be constructed based on the admittance matrix. This ensures consistency and seamless integration with EMT simulations, allowing accurate representation and analysis of the grounding system behavior in EMT studies.

First, the input is determined in terms of the output:

$$y = C.x + D.u \Rightarrow Du = y - C.x \Rightarrow$$
$$u = D^{-1}(y - C.x) \Rightarrow u = -D^{-1}C.x + D^{-1}.y \quad (15)$$

As another representation:

$$\dot{x} = A.x + Bu \Rightarrow \dot{x} = Ax + B(D^{-1}y - D^{-1}Cx)$$
$$\Rightarrow \dot{x} = (A - B.D^{-1}C)x + BD^{-1}y \quad (16)$$

Therefore, the state-space matrices can be obtained as:

$$\dot{x}(t) = A_{new}.x(t) + B_{new}.v(t)$$
$$i(t) = C_{new}.x(t) + D_{new}.v(t) \quad (17)$$

where,

$$A_{new} = A - B.D^{-1}C \quad B_{new} = \mathrm{B}.D^{-1}$$
$$C_{new} = -D^{-1}C \quad D_{new} = D^{-1} \quad (18)$$

It should be noted that we use an analytical formula for considering the frequency dependence of soil electrical parameters. This model satisfies causality and is obtained considering in-situ experiments that was recently recommended by CIGRE [25] for lightning-related studies as follows:

$$\sigma_g(f) = \sigma_0 + \sigma_0 \times h(\sigma_0)(f \times 10^{-6})^{£}$$
$$\varepsilon_{rg}(f) = \varepsilon_{r\infty} + \frac{tan\left(\frac{\pi £}{2}\right)\times 10^{-3}}{2\pi\varepsilon_0(10^6)^{£}}\sigma_0 \times h(\sigma_0)(f)^{£-1} \quad (19)$$

where f (Hz) is the frequency, σ_g (mS/m) and σ_0 (mS/m) are the soil conductivity and DC conductivity, respectively; ε_{rg} (F/m) and $\varepsilon_{r\infty}$ (F/m) are, respectively, the relative permittivity and the relative permittivity at higher frequencies.

To represent a more accurate grounding system, a two-layer soil is considered by an upper layer with a finite depth above a lower layer with an infinite depth (see further details in [26]).

4. Simulation results

To investigate the effects of FD modeling of GS and PEEC modeling of PVs on lightning-generated overvoltages, the test solar system is simulated in EMTP. The test system consists of four PV arrays containing 10 PV panels. The capacity of each panel is 350 W with a total output of 3.5 kW and occupying an area of 5 m × 4 m. The zoom-in view of the cross section of solar frame is shown in Figure 3. The solar frame has a width of 1 m and a length of 2 m. Moreover, the cross-section of the frame has a width of 2 cm and a height of 5 cm.

The test system is simulated for two different scenarios namely end-grounded and middle-grounded. In the case of end-grounded test, the grounding grid is connected to one end of the four arrays, while in the middle-grounded scenario; the grounding grid is connected to the mid-point of each of the four arrays as shown in Figure 4.

This study analyzes the effects of GS modeling on the generated overvoltages on the PV test system due to the direct lightning strikes at point A (Figure 4). The lightning return stroke is modeled using the Heidler function as [27]:

$$i(t)=\frac{I_p}{\eta}\frac{k^n}{1+k^n}e^{\frac{-t}{t_2}} \qquad (20)$$

The lightning channel impedance is considered 400 Ω [28]. The GS is analyzed for three different soil resistivities, i.e., ρ=10, 100, and 1000 Ωm. In these analyses, it is assumed that the value of relative permittivity ε_r is equal to 20.

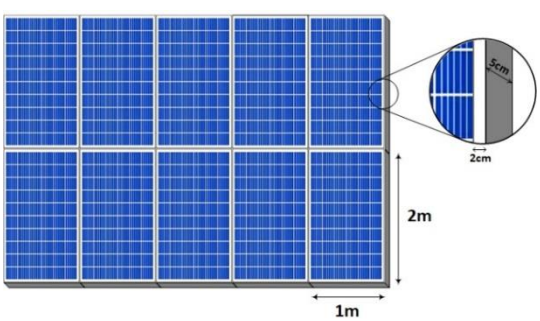

Figure 3. PV assembly

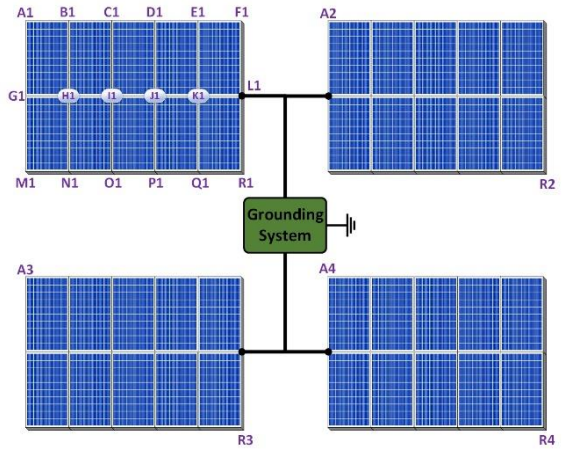

(a)

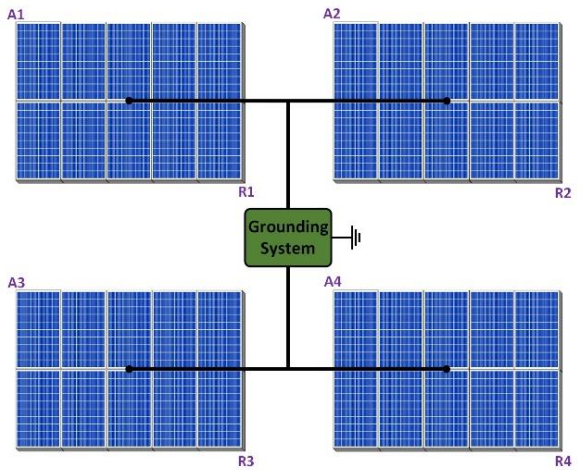

(b)

Figure 4. Solar PV assembly. (a): end-grounded, (b): middle-grounded grounding system

The end-grounded and middle-grounded GSs are connected to two different electrodes: 1) a 3-meter vertical grounding electrode (single-port GS); 2) a 6m*6m square grid grounding buried at a depth of 1 m (4-port GS), as shown in Figure 5.

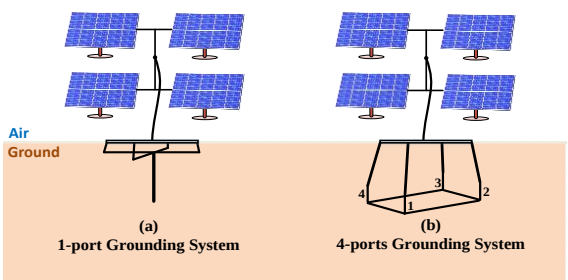

Figure 5. Grounding systems, (a) 3-meter vertical rod, and (b) 6 m×6 m square grid.

4.1. Verification of the Model

The results obtained by simulating the proposed method for the PV module and grounding electrodes are compared with the experimental data reported in [21]. The experimental parameters of PV systems and GSs are presented in Table 1. The voltages of legs 1 and 3 at the bottom points are demonstrated in Figure 6 (upper and lower panels, respectively). It is noted that the external grounding resistance is considered to be 2.2 Ω. Note that for avoiding soil ionization, low value of impulse current is injected into the test case.

To get a highly accurate results, all factors including: the mounting system, PV frame, and mutual coupling are considered in the PV module modeling. Moreover, the FD wide-band model is used for the GSs. It can be seen that the proposed modeling results are in good agreement with the measured data. The validated results ensure that the proposed models can be implemented for large-scale PV systems.

Table 1. Experimental parameters for PV and soil

PV module	Maximum power	Open circuit voltage	Short circuit current	Dimensions
	285 W	38.7 V	9.42 A	1640*992935 mm
Mounting system of PV	Front legs (Two)	Rear legs (Two)	Cross grider	Rear grider
	250	600	1000	1000
Soil and Lightning current	Type of GS	External resistance	Relative permittivity	Impulse voltage
	vertical	2.2Ω	10	10kV/0.2μs/ 0.6μs

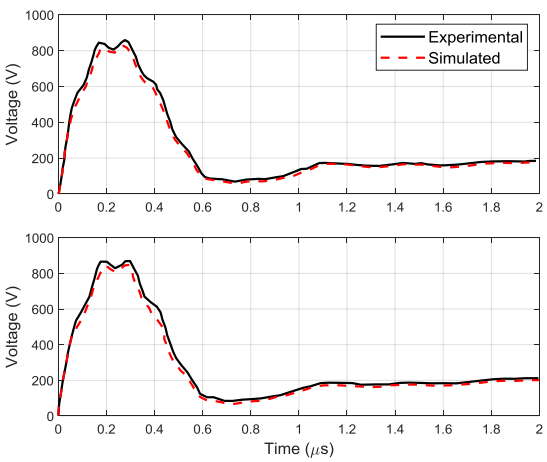

Figure 6. Transient voltages caused by low magnitude impulse current

Table 2. Two-norm cumulative relative error comparison

Modeling methods	Points of voltage values	
	Leg 1	Leg 3
Simulated vs experimental results	2.574e-4	3.149e-4

Table 2 shows the 2-norm error computed for voltages of legs 1 and 3. As can be observed, the precision of the proposed model is very close to experimental data.

4.2. Influence of two-layer soil

In order to compare the effects of upper layer depth and soil resistivity of layers, Table 3 summarizes Ground Potential Rise (GPR) for a vertical electrode. The soil resistivity for top layer is $\rho_1 = 100$ Ωm, while for the lower layer considered to be $\rho_2 = 10$, 100 and 1000 Ωm, so the reflection factors are K= -0.9, 0 and 0.81, respectively.

It is clear that the upper layer length has a significant impact on GPR. As an example, in the case of negative reflection (K=-0.9), the GPR increases with increasing upper layer length, while the relation of overvoltages for positive reflection is opposite to that case.

Table 3. GPR (kV) for a vertical electrode with 30 kA lightning current

Reflection factor	Upper layer length (m)			
	1	10	100	1000
K = -0.9	425	970	1640	1700
K = 0	1700	1700	1700	1700
K = 0.81	4030	2820	1760	1700

4.3. Influence of wide band modeling of GSs

To analyze the influence of the FD modeling of GS on the calculated overvoltages, a sensitivity analysis was performed for the solar test case of Figure 4.

The generated voltages at point A are shown in Figures 7 and 8 for the static (ST) and FD wide-band modeling. It is worth mentioning that a 3-meter vertical rod is used for Figure 7, and square grid GSs are applied for Figure 8. Here, middle- and end-grounded grids are used for both cases with low and high soil resistivities.

According to Figure 7, the lightning-induced overvoltages increase with an increase in the soil resistivity for both middle- and end-grounded grids. In all cases, the maximum voltages for static modeling of GS are higher than those for the FD

wide-band modeling. However, this difference is more significant in the case of soil with high resistivity, ρ=1000 Ωm. It is obvious that in the group of arrays with end-grounded grids, the potential drop at the point of lightning strike is about 30% higher than that in the middle-grounded grids.

It is observed in Figure 8 that the generated overvoltages increase with increasing soil resistivity in the case of square grid grounding. From Figure 8, in soil with ρ=100 Ωm, the overvoltage in the static model is lower than that in the FD wide-band model due to the inductive behavior of GS, while in soil with ρ=1000 Ωm, the overvoltage in static model is higher than that in FD wide-band model due to the capacitive behaviour of GS. As an example, the value of overvoltage in the static model is 1290 kV, about 4% less than that in the FD wide-band model, for the end-grounded grid with ρ=100 Ωm.

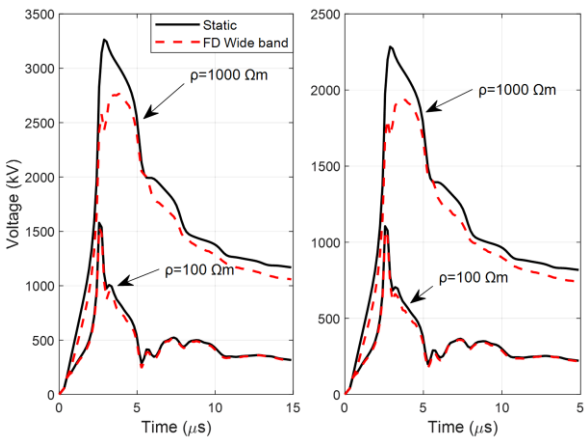

Figure 7. Overvoltages at point *A*. Left panel: end-grounded and right panel: middle-grounded grids, using 3-meter vertical rod.

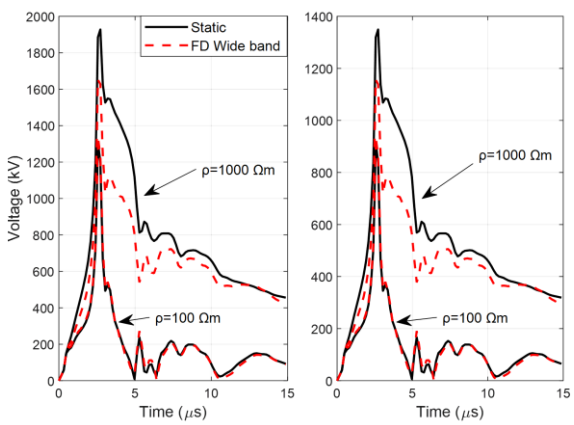

Figure 8. Overvoltages at point *A*. Left panel: end-grounded and right panel: middle-grounded grids, using square grid GS.

The overvoltage magnitude in the static model is 1940 kV, about 15% higher than that in the frequency dependent model, for ρ=1000 Ωm. It is also clear that the voltage values of the end-grounded structure are around 30% higher than those of the middle-grounded structure, similar to the vertical rod GS.

4.4. Influence of lightning current parameters

To evaluate the electromagnetic transient effect of lightning strikes on solar PV, the variation of return stroke parameters and soil resistivity must be studied accurately. The maximum voltage on the output wire is due to the variations of lightning peak values and soil resistivities, as shown in Figures 9 and 10, respectively. The overvoltage values during the lightning strike are calculated at four different points (*A*, *H*, *J*, and *L* in Figure 4).

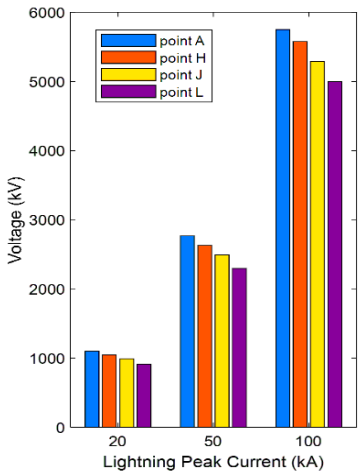

(a)

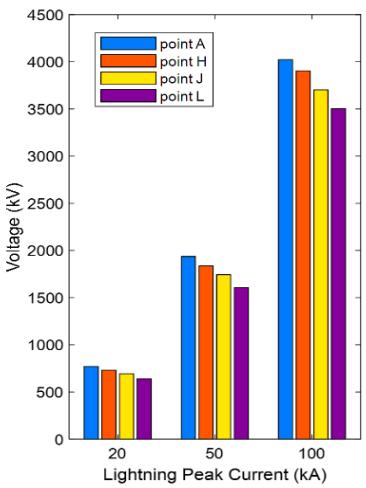

(b)

Figure 9. Peak values of overvoltage with the peak lightning current; (a): end-grounded, (b): middle-grounded grids.

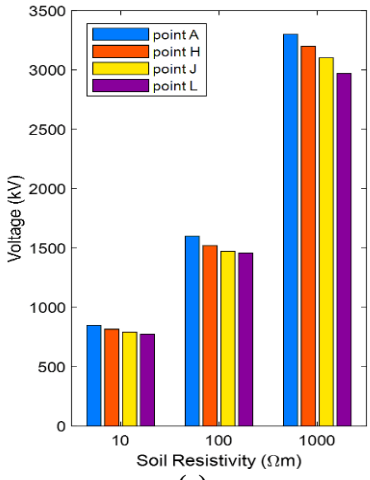

(a)

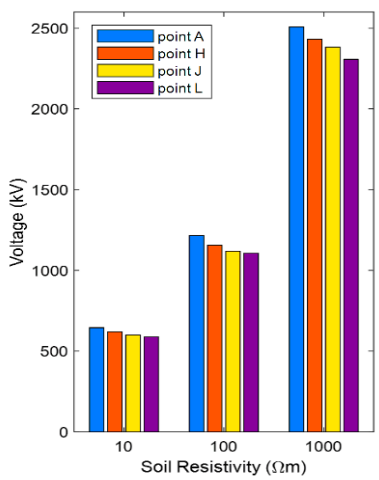

(b)

Figure 10. Peak values of overvoltage with the soil resistivities; (a): end-grounded, (b): middle-grounded grids.

According to Figure 9, the overvoltage peak values increase with the increase in lightning current peak value. Furthermore, it is obvious that the maximum voltage gradually decreases by approaching the ground (point *A* toward *L*). It is worth mentioning that the voltages of the rest of the PV arrays at points *A*, *H*, *J*, and *L* are similar.

According to Figure 10, the maximum voltage rises as the soil resistivity increases for both end-grounded and middle-grounded GSs. Additionally, when the middle-grounded grid configuration is employed, the overvoltage values are lower compared to the scenario with the end-grounded grid. This suggests that using a middle-grounded grid configuration can help mitigate overvoltage issues and provide improved protection in terms of voltage levels, particularly under higher soil resistivity conditions.

4.5. Influence of PV factors

In the PV systems, the structure of the mounting system, mutual coupling, and metal frame as well as the location of the grounding legs, have a significant impact on the distribution of lightning current.

To analyze the effects of the PV frame, mounting system, and mutual coupling on the value of the generated voltage at point *A* of array 1, a sensitivity analysis is performed. Figure 11 shows the overvoltages at point *A* in the case of a direct lightning strike at point *A*. In this figure, if the effects of mutual coupling, metal frame, and mounting system are considered, the results are labeled "With PV factors", while if the effects are ignored, the results are labeled "Without PV factors".

It is observed that considering the mounting system, metal frame, and mutual coupling has a huge impact on the generated voltages. It can be seen that these factors increase the obtained overvoltage values by 25% for the case of low soil resistivity and up to 35% for the case of high resistivity, i.e., ρ=1000 Ωm.

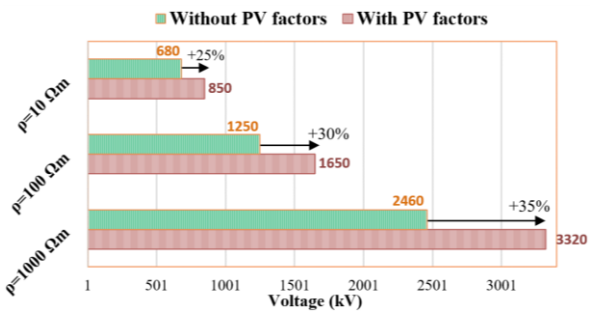

Figure 11. Generated overvoltage at point *A*.

5. Conclusions

Solar PV panels are exposed to lightning strikes, which can affect the performance and life cycle of the panels. Most EMT tools, such as EMTP, ATP and PSCAD/EMTDC, are based on Dommel's approach, so to evaluate the FD impedance of GSs in EMT solvers, the impedance matrix needs to be inverted in conventional methods. This matrix inversion requires some approximations at low frequencies in the case of multi-port GSs. The PEEC method was used to model a PV system considering the mounting system, PV module frame, and mutual coupling effects. Based on the simulation results, it was shown that the FD wide-band modeling for the PV panel and GS systems significantly affects lightning-generated overvoltage. Consequently, this modeling can substantially influence the design of lightning protection systems from both economic and technical

aspects. Notably, the proposed method exhibits advantages over previous approaches in terms of both accuracy and complexity, making it a favorable choice for both single-port and multi-port grounding grids. The improved accuracy and reduced complexity of the proposed method make it a valuable tool for enhancing the design and performance of lightning protection systems. The results showed that middle-grounded arrays have lower voltage values compared to end-grounded ones. Hence, it is reasonable to take into account these arrays for achieving proper GS structures. The validated results ensure that the proposed GSs and PV models can be applied in large-scale PV systems. However, further work is required to model grounding system considering both frequency dependence and soil ionization behavior.

Nomenclature

Abbreviation

PV	Photovoltaic
EMT	Electromagnetic Transient
GS	Grounding Systems
FD	Frequency-Dependent
WB	Wide-Band
PEEC	Partial Element Equivalent-Circuit Method
MoM	Method of Moments
VF	Vector Fitting

Symbols

σ	Conductivity (S/m)
ρ	Soil resistivity
μ_0	Permeability of vacuum ($4\pi \times 10^{-7}$ H·m^{-1})
ε_0	Permittivity of vacuum (8.854×10^{-12} F/m)
ε_r	Relative permittivity
σ	Conductivity
f_c	Upper cutoff frequency
η	Intrinsic impedance

Parameters

R	Resistance
L	Inductance
C	Capacitance
P_{jk}	coefficient matrix
l_i	Length of conductor i
l and m	Lengths of conductors j and k
d	Diameter of vertical electrode
r	Radius of conductor
δ	Skin depth
θ	Angle difference between two conductors
$Z(s)$	Impedance matrix of grounding system
$Y(s)$	Admittance matrix of grounding system
$\boldsymbol{x}(t)$	State vector
$\boldsymbol{v}(t)$	Vector of voltage
$\boldsymbol{i}(t)$	Vector of current

References

[1] Patanik, S., Guru, N., Kasturi, K., & Nayak, M. R. (2023). Solar Photovoltaic and Wind Turbine Generation based Microgrid Management Architecture Considering Battery Energy Storage Degradation and Time of Use Tariff. *Journal of Solar Energy Research*, *8*(2), 1459-1470. DOI: 10.22059/jser.2023.356135.1276

[2] Ghaffarzadeh, N., & Faramarzi, H. (2022). Optimal Solar plant placement using holomorphic embedded power Flow Considering the clustering technique in uncertainty analysis. *Journal of Solar Energy Research*, *7*(1), 997-1007. DOI: 10.22059/jser.2022.330961.1221

[3] Perera, T., & Udayakumar, C. (2023). Voltage Unbalance Assessment of Solar PV Integrated Low Voltage Distribution System in Sri Lanka Using Monte Carlo Simulation. *Journal of Solar Energy Research*, *8*(2), 1357-1366. DOI: 10.22059/jser.2023.350730.1262

[4] Aryan Nezhad, M. (2022). Frequency control and power balancing in a hybrid renewable energy system (HRES): Effective tuning of PI controllers in the secondary control level. *Journal of Solar Energy Research*, *7*(1), 963-970. DOI: 10.22059/jser.2022.330109.1219

[5] Chatterjee, S., Kumar, P., & Chatterjee, S. (2018). A techno-commercial review on grid connected photovoltaic system. *Renewable and Sustainable Energy Reviews*, *81*, 2371-2397. DOI: 10.1016/j.rser.2017.06.045

[6] Hussein Sachit, A., Fani, B., Delshad, M., Shahgholian, G., & Golsorkhi Esfahani, A. (2023). Analysis and Implementation of Second-Order Step-Up Converter Using Winding Cross Coupled Inductors for Photovoltaic Applications. *Journal of Solar Energy Research*, *8*(2), 1516-1525. DOI: 10.22059/JSER.2023.357285.1291

[7] Hernández, Y. M., Tsovilis, T. E., Asimakopoulou, F., Politis, Z., Barton, W., & Lozano, M. M. (2016). A simulation approach on rotor blade electrostatic charging and its effect on the lightning overvoltages in wind parks. *Electric Power Systems Research*, *139*, 22-31. DOI: 10.1016/j.epsr.2015.11.039

[8] Hernandez, J. C., Vidal, P. G., & Jurado, F. (2008). Lightning and surge protection in

photovoltaic installations. *IEEE Transactions on power delivery*, *23*(4), 1961-1971. DOI: 10.1109/TPWRD.2008.917886

[9] Staikos, E. T., Peppas, G. D., & Tsovilis, T. E. (2022). Wide Frequency Response of Varistors and Coordination With Transient Voltage Suppression Diodes. *IEEE Transactions on Power Delivery*, *38*(1), 453-462. DOI: 10.1109/TPWRD.2022.3194595

[10] Zhang, Y., Chen, H., & Du, Y. (2020). Considerations of photovoltaic system structure design for effective lightning protection. *IEEE Transactions on Electromagnetic Compatibility*, *62*(4), 1333-1341. DOI: 10.1109/TEMC.2020.2990930

[11] Konneh, K. V., Masrur, H., Othman, M. L., Wahab, N. I. A., Hizam, H., Islam, S. Z., ... & Senjyu, T. (2021). Optimal design and performance analysis of a hybrid off-grid renewable power system considering different component scheduling, PV modules, and solar tracking systems. *IEEE Access*, *9*, 64393-64413. DOI: 10.1109/ACCESS.2021.3075732

[12] Demirel, E., Dolgun, G. K., & Keçebaş, A. (2022). Comprehensive transient analysis on control system in a photovoltaic power plant under lightning strike. *Solar Energy*, *233*, 142-152. DOI: 10.1016/j.solener.2022.01.037

[13] Sueta, H. E., Modena, J., Barbosa, J. O., Santos, S. R., & Zilles, R. (2022, October). Preliminary studies on the distribution of lightning current in the components of PV modules. In *2022 36th International Conference on Lightning Protection (ICLP)* (pp. 1-6). IEEE. DOI: 10.1109/ICLP56858.2022.9942591

[14] Azamian, A., Rezaeealam, B., Ghanbari, T., & Rokrok, E. (2023). Improved Low Voltage Ride-through Capability of PV Connected to the Unbalanced Main Grid. *Journal of Solar Energy Research*, *8*(1), 1326-1344. DOI: 10.22059/jser.2022.351322.1264

[15] Sun, Q., Zhong, X., Huang, L., & Yao, L. (2022). A Novel Crossover Wiring of DC Cable for Photovoltaic System Against Lightning-Induced Overvoltage. *IEEE Transactions on Electromagnetic Compatibility*. DOI: 10.1109/TEMC.2022.3227365

[16] Naxakis, I., Nikolaidis, P., & Pyrgioti, E. (2016, September). Performance of an installed lightning protection system in a photovoltaic park. In *2016 IEEE International Conference on High Voltage Engineering and Application (ICHVE)* (pp. 1-4). IEEE. DOI: 10.1109/ICHVE.2016.7800672

[17] Zhang, Y., Chen, H., & Du, Y. (2019). Lightning protection design of solar photovoltaic systems: Methodology and guidelines. *Electric Power Systems Research*, *174*, 105877. DOI: 10.1016/j.epsr.2019.105877

[18] Hetita, I., Zalhaf, A. S., Mansour, D. E. A., Han, Y., Yang, P., & Wang, C. (2022). Modeling and protection of photovoltaic systems during lightning strikes: A review. *Renewable Energy*, *184*, 134-148. DOI: 10.1016/j.renene.2021.11.083

[19] Zhang, Y., Chen, H., & Du, Y. (2020). Considerations of photovoltaic system structure design for effective lightning protection. *IEEE Transactions on Electromagnetic Compatibility*, *62*(4), 1333-1341. DOI: 10.1109/TEMC.2020.2990930

[20] Wang, Y., Yao, X., Tao, S., Zhang, X., Lin, Y., & Sua, M. (2020). Study on lightning transient behavior of photovoltaic installations. *Int. J. Smart Grid Clean Energy*, *9*(2), 390-396. DOI: 10.12720/sgce.9.2.390-396

[21] Hetita, I., Mansour, D. E. A., Han, Y., Yang, P., & Zalhaf, A. S. (2022). Experimental and numerical analysis of transient overvoltages of PV systems when struck by lightning. *IEEE Transactions on Instrumentation and Measurement*, *71*, 1-11. DOI: 10.1109/TIM.2022.3199225

[22] Alemi, M. R., & Sheshyekani, K. (2015). Wide-band modeling of tower-footing grounding systems for the evaluation of lightning performance of transmission lines. *IEEE Transactions on Electromagnetic Compatibility*, *57*(6), 1627-1636. DOI: 10.1109/TEMC.2015.2453512

[23] Morched, A., Gustavsen, B., & Tartibi, M. (1999). A universal model for accurate calculation of electromagnetic transients on overhead lines and underground cables. *IEEE Transactions on Power Delivery*, *14*(3), 1032-1038. DOI: 10.1109/61.772350

[24] Gustavsen, B., Martinez, J. A., & Durbak, D. J. I. T. O. P. D. (2005). Parameter determination for modeling system transients-Part II: Insulated cables. *IEEE Transactions on power delivery*, *20*(3), 2045-2050. DOI: 10.1109/TPWRD.2005.848774

[25] Cigré, W. G. (2019). Impact of Soil-Parameter Frequency Dependence on the Response of Grounding Electrodes and on the Lightning Performance of Electrical Systems (C4. 33). *Technical Brochure*, *67*.

[26] Permal, N., Osman, M., Ariffin, A. M., & Ab Kadir, M. Z. A. (2021). The impact of substation grounding grid design parameters in non-homogenous soil to the grid safety threshold parameters. *IEEE Access*, *9*, 37497-37509. DOI: 10.1109/ACCESS.2021.3063018

[27] Heidler, F., Cvetic, J. M., & Stanic, B. V. (1999). Calculation of lightning current parameters. *IEEE Transactions on power delivery*, *14*(2), 399-404. DOI: 10.1109/61.754080

[28] Datsios, Z. G., Mikropoulos, P. N., & Tsovilis, T. E. (2019). Effects of lightning channel equivalent impedance on lightning performance of overhead transmission lines. *IEEE Transactions on Electromagnetic Compatibility*, *61*(3), 623-630. DOI: 10.1109/TEMC.2019.2900420